Mixing and Particle Dispersion in the Wavy Vortex Regime of Taylor–Couette Flow

Murray Rudman
CSIRO Building, Construction and Engineering, Highett, Graham Road, Victoria 3190, Australia

Fluid flow and particle dispersion were investigated numerically in the wavy vortex regime of Taylor–Couette flow. The flow field for wavy vortex flow is stationary when viewed in a frame rotating with the azimuthal wave velocity. These steady flow fields are used to track fluid particles and to estimate the effective axial diffusion resulting from chaotic fluid advection. The effective diffusion coefficient for a fixed wave state is a function of the Reynolds number. Particle dispersion is a strong function of wave state, showing that a universal relationship between dispersion and Reynolds number cannot be found in this regime of cylindrical Taylor–Couette flow. The effective Schmidt number of chaotic advection is less than unity for all wavy vortex flows examined, indicating that chaotic advection plays an important role in fluid mixing in these flow regimes. Fluid particle retention in the cores of the wavy vortices is also predicted for some parameter regimes, although not all. Particles trapped in vortex cores are only poorly mixed within the core and play no role in global mixing. A preliminary examination of inertial particle settling suggests that the fluid flow does not prevent settling in the mean, although the magnitude of the settling velocity significantly affects the dispersion of inertial particles.

Introduction

Cylindrical Taylor–Couette flow occurs between two concentric cylinders, one or both of which is allowed to rotate in either the same or opposite directions. Cylindrical Taylor–Couette vessels have been used both as reaction vessels and to quantify the relationship between shear and aggregation by coagulation or flocculation (Ives and Al Dibouni, 1979; Hoare et al., 1982; Stein et al., 1986; Tsai et al., 1987; Pudjiono and Tavare, 1993; Farrow and Swift, 1996). Pudjiono et al. (1992) describe other applications for cylindrical Taylor–Couette flow, including viscometry, cooling of rotating electrical machinery, dynamic filtration and classification, electrolytic applications, and catalytic chemical reactors. Apart from its many practical applications, it is a flow of fundamental fluid dynamical importance and has been extensively studied since the work of Taylor (1923).

The range of different Taylor–Couette flow regimes and their dependence on inner and outer rotation rates is complex. The most complete study of flow regimes is given by Andereck et al. (1986), in which flow types observed in their column are classified into eighteen principal regimes. When only the inner cylinder rotates, a critical Reynolds number, Re_C, exists at which cylindrical Couette flow becomes unstable to axial perturbations. The resulting flow consists of a series of laminar, counterrotating toroidal vortices with azimuthal symmetry. This flow, usually termed Taylor vortex flow, is a steady two-dimensional flow, and fluid elements are constrained to lie on invariant tori within vortices. Apart from molecular diffusion, each vortex remains disconnected from its neighbors and because of this, the vortex cores are not efficient mixers. When axisymmetric Taylor vortex flow is considered as a chemical-reaction system, each vortex is often described as being a well-mixed reactor that is disconnected with all others in the system (Kataoka et al., 1975; Pudjiono and Tavare 1993). Because the flow is steady and two-dimensional, mixing within each vortex is limited by molecular diffusion.

As the Reynolds number is increased beyond Re_C, a point is reached at which Taylor vortex flow becomes unstable to azimuthal perturbations. The resulting "wavy vortex flow," in which an azimuthal traveling wave propagates around the Taylor vortices, is the subject of this article. In an analysis of an analytic approximation to Taylor–Couette flow, Broomhead and Ryrie (1988) showed that quite small deviations from steady two-dimensional vortex flow could cause fluid trajectories to become chaotic, thus suggesting that fluid mixing in this flow regime is enhanced considerably. Azimuthal pertur-

bations with an amplitude as small as 5% of the inner cylinder velocity were sufficient to ensure that most regions of their flow became well mixed. Because waviness breaks the symmetry of Taylor vortex flow, true wavy vortex flow may be expected to give rise to chaotic particle motion and hence far better mixing than Taylor vortex flow.

In chemically reacting systems, chaotic flows have distinct advantages over nonchaotic, the most important being the relative rapidity with which reactants become well-mixed. This point is especially important for fast reactions in which the reaction time scale is much smaller than the diffusion time scale and the reaction occurs only on the surface separating the reacting components. To ensure a fast reaction, the rapid creation of as much surface area between the reactants as possible is essential, and chaotic mixing enhances the rate of surface-area creation [see chap. 9 of Ottino (1989) for a discussion of these issues]. For slow reactions, residence-time theory is often adequate, and the approach of Kataoka et al. (1975) for axisymmetric vortex flow is an appropriate approximation.

Although there have been many studies of mixing in periodic cellular flow fields (e.g., Solomon and Gollub, 1988; Broomhead and Ryrie, 1988; Weiss and Knobloch, 1989; Cox et al., 1990; Ryrie, 1992; Ashwin and King, 1997), there are few studies that consider fully nonlinear, three-dimensional solutions of the Navier–Stokes equations in flow regimes far from two-dimensionality. This study extends previous model studies of nonaxisymmetric Taylor–Couette flows by using such solutions of the Navier–Stokes equations. Although justified on this ground alone, it also allows an understanding to be gained of mixing in a flow that is of practical chemical engineering importance. Consideration of fully nonlinear wavy vortex flows is particularly relevant because of the limited range of rotation rates that result in axisymmetric Taylor vortex flow, and the considerably larger range that admits wavy vortex solutions.

The overall goal of this article is to examine the effect of waviness on particle transport in Taylor–Couette flow. To this end, several specific aims are considered, each of which is addressed using numerical solutions of the fluid flow and trajectories of fluid elements (or inertial particles) through a section of a cylindrical Taylor–Couette vessel of theoretically infinite axial extent. The first aim is to investigate dispersion (and to suggest its consequences for mixing) while varying Re, and to see if a functional relationship between dispersion and Re can be obtained. The second aim relates to the observation of Coles (1965) that for a given value of Re_I in the wavy vortex regime, many different wave states can exist. Thus the effect of wave state on dispersion is considered. Finally, because cylindrical Taylor–Couette vessels are often used in situations in which small heavy particles are formed (e.g., Tsai et al., 1987; Farrow and Swift, 1996), a preliminary investigation of the interaction between wavy vortex flow and the settling of small inertial particles is presented.

Although the effect of radius ratio, η, on dispersion is also of considerable interest, it is not addressed here. The only value of η considered is $\eta = 0.874$, which corresponds to the cylindrical Taylor–Couette vessel used in the experimental study of Coles (1965). Coles presents detailed results of accessible wave states and wave velocities for this radius ratio, and this information is beneficial for numerical validation.

Numerical Method

The numerical procedures used to quantify dispersion are broken into two distinct parts. First, the unsteady solution of the fluid-flow field is obtained in a stationary coordinate frame using the conservative fluid difference method detailed below. Second, the fluid-flow solution is used to integrate both fluid trajectories and inertial particle trajectories forward in time. Although the flow is unsteady in a stationary coordinate frame, in the wavy vortex regime, the flow field is steady when viewed in a coordinate frame that rotates with the angular velocity of the azimuthal wave. The stationarity of the fluid flow in this frame is essential for the efficient solution of the particle-trajectory problem. If a fully unsteady fluid-flow solution were to be coupled to the time integration of particle trajectories, examination of more than a few different cases would be prohibitively expensive with current computer resources. This is the main reason that modulated wavy vortex flow is not considered here—another reason being the requirement that the full azimuth of the vessel must be considered if the m-fold symmetry of wavy vortex flow is broken by a modulating azimuthal frequency with a different wave number.

Fluid-flow solution

The Navier–Stokes equations are written in cylindrical coordinates and are nondimensionalized with the velocity of the inner cylinder ($V_I = \Omega_I R_I$), the distance between inner and outer cylinders (or gap width) d, and the kinematic viscosity ν. They are written:

$$\frac{\partial U}{\partial t} + \frac{1}{r}\frac{\partial (rU^2)}{\partial r} + \frac{1}{r}\frac{\partial (VU)}{\partial \theta} - \frac{V^2}{r} + \frac{\partial (WU)}{\partial z} = -\frac{\partial P}{\partial r} + \frac{1}{Re}\left[\frac{\partial}{\partial r}\left(\frac{1}{r}\frac{\partial rU}{\partial r}\right) + \frac{1}{r^2}\frac{\partial^2 U}{\partial \theta^2} - \frac{2}{r^2}\frac{\partial V}{\partial \theta} + \frac{\partial^2 U}{\partial z^2}\right] \quad (1)$$

$$\frac{\partial V}{\partial t} + \frac{1}{r}\frac{\partial (rUV)}{\partial r} + \frac{1}{r}\frac{\partial V^2}{\partial \theta} + \frac{(UV)}{r} + \frac{\partial (WU)}{\partial z} = -\frac{\partial P}{\partial \theta} + \frac{1}{Re}\left[\frac{\partial}{\partial r}\left(\frac{1}{r}\frac{\partial rV}{\partial r}\right) + \frac{1}{r^2}\frac{\partial^2 V}{\partial \theta^2} + \frac{2}{r^2}\frac{\partial U}{\partial \theta} + \frac{\partial^2 V}{\partial z^2}\right] \quad (2)$$

$$\frac{\partial W}{\partial t} + \frac{1}{r}\frac{\partial (rUW)}{\partial r} + \frac{1}{r}\frac{\partial (VW)}{\partial \theta} + \frac{\partial W^2}{\partial z} = -\frac{\partial P}{\partial z} + \frac{1}{Re}\left[\frac{1}{r}\frac{\partial}{\partial r}\left(r\frac{\partial W}{\partial r}\right) + \frac{1}{r^2}\frac{\partial^2 W}{\partial \theta^2} + \frac{\partial^2 W}{\partial z^2}\right] \quad (3)$$

$$\frac{1}{r}\frac{\partial rU}{\partial r} + \frac{1}{r}\frac{\partial V}{\partial \theta} + \frac{\partial W}{\partial z} = 0, \quad (4)$$

where U is the radial velocity (positive away from the centerline); V is the azimuthal velocity (positive in an anticlockwise sense); W is the axial velocity; and the Reynolds number is $Re = \Omega_I R_I d/\nu$. Important to note when tracking of inertial particles is considered is that the pressure P in Eqs. 1–3 is a dynamic pressure and does not contain a contribution from the gravitational acceleration. Gravity can be neglected in the fluid-only solution, as it plays no role, although it must be

correctly incorporated in the particle equations for inertial particles.

The equations are discretized on a uniform, staggered mesh (Welch et al., 1965), with discrete pressures P defined at cell centers (i, j, k) and grid velocities defined at the centers of cell faces, $U_{i+(1/2),j,k}$, $V_{i,j+(1/2),k}$, and $W_{i,j,k+(1/2)}$.

Time integration of the discrete equations is by an improved Euler scheme that is second-order accurate in time. Given the values of $P^n_{i,j,k}$, $U^n_{i+(1/2),j,k}$, $V^n_{i,j+(1/2),k}$ and $W^n_{i,j,k+(1/2)}$, the time-stepping algorithm is described by first considering a first-order explicit algorithm that consists of the following steps:

- Find intermediate values of the velocity field based on old values of the velocity and pressure:

$$U^* = U^n + \delta t(-\mathfrak{A}(U^n) - \nabla P^n + \mathfrak{D}(U^n)),$$

where $U = (U, V, W)$, and the symbols $\mathfrak{A}$ and $\mathfrak{D}$ refer to the advective and diffusive operators, respectively.

- Calculate the pressure correction, δP, from the discrete form of the following Poisson equation:

$$\nabla^2 \delta P = \frac{1}{\delta t} \nabla \cdot U^*.$$

- Find the $(n+1)$ estimates of velocity and pressure:

$$U^{n+1} = U^* - \delta t \nabla \delta P \qquad P^{n+1} = P^n + \delta P.$$

The second-order in time algorithm performs the preceding three steps twice: the first time with a half time-step to estimate values of $U^{n+(1/2)}$ and $P^{n+(1/2)}$; the second time with a full time-step, but with the advective, diffusive, and pressure terms on the righthand side calculated using $U^{n+(1/2)}$ and $P^{n+(1/2)}$.

The advective operator $\mathfrak{A}$ is discretized using a third-order in-space version of the QUICK scheme of Leonard (1979), and the diffusive terms $\mathfrak{D}$ are discretized using second-order centered spatial differences. The pressure algorithm just given is based on that first discussed by Amsden and Harlow (1970), and the resulting Poisson equation for the pressure correction, δP, is solved using a defect-correction multigrid technique similar to that discussed in Morton et al. (1995).

Computational parameters

The wave state existing in the vessel in the wavy vortex regime may be categorized with a wave-number pair (m, n). The number of periods in the azimuth is defined by m (giving an azimuthal wavelength of $2\pi/m$ rad), and the number of pairs of vortices in the axial direction is defined by n. The gapwidth in Coles' (1965) experiment was 0.72 in., and the axial extent was 20.09 in. (510.3 mm), thus the axial wavelength is defined to be $20.09/(0.72n)$ or $27.9/n$ gapwidths.

The geometry of the computational domain is shown in Figure 1. The radial extent, d, is one gapwidth, the azimuthal extent, Θ, is $2\pi/m$ rad, and the axial extent, λ_z, is $27.9/n$ times the gapwidth. The axial boundaries are periodic, as are the azimuthal boundaries. The inner radial boundary (at a radius of 6.9444 gapwidths) rotates with a scaled velocity of 1.0 and the outer radial boundary is stationary. Thus the

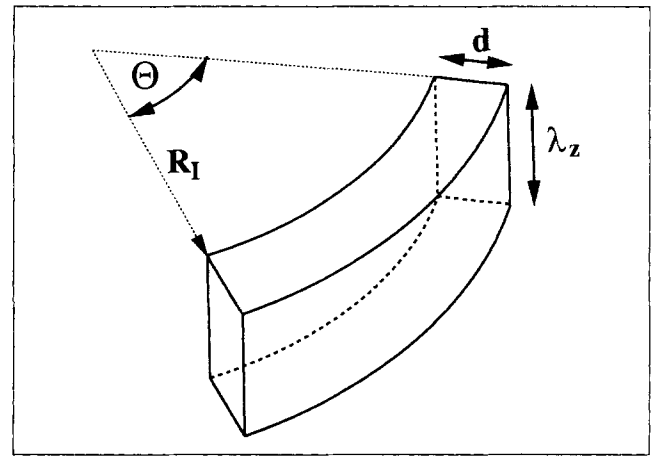

Figure 1. Computational domain of one gapwidth d in the radial direction, $\lambda_z = 27.9/n$ gapwidths in the axial direction, and $2\pi/m$ rad in the azimuthal direction.

Boundary conditions are periodic in both θ and z.

computational domain represents just one oscillation of the wavy vortex flow in the axial and azimuthal directions. This geometry therefore restricts the possible solutions to those cases in which these two periodicities are strictly realizable—that is, to the wavy vortex flow regime.

The fluid-flow solution is integrated forward in time until a state is reached in which the period, τ, of the azimuthal wave is constant. The period is defined to be the time taken for the wave to travel an angular distance of $2\pi/m$ rad, and the frame in which the flow appears stationary is one that rotates with a constant angular velocity of $\Omega_\tau = 2\pi/m\tau$.

Fluid-particle trajectories

In the frame of the azimuthal wave, fluid-particle trajectories are calculated from the following equations:

$$\frac{dr_p}{dt} = U_f$$

$$\frac{d\theta_p}{dt} = \frac{V_f}{r_p} - \Omega_\tau$$

$$\frac{dz_p}{dt} = W_f, \tag{5}$$

where the subscript p refers to a fluid particle and f refers to the fluid velocity at this location. The systems of equations are integrated forward in time using a fourth-order Runge-Kutta method (RK4). Velocities are required at particle positions and are obtained from the fluid velocity field using quadratic interpolation.

Numerical Validation

To estimate the resolution required for a converged solution, the fluid-flow solution for $Re_I = 648$, $(m, n) = (6, 12)$ was calculated at grid resolutions of $12 \times 24 \times 24$, $16 \times 32 \times 32$, $24 \times 48 \times 48$, and $32 \times 64 \times 64$. The period of the azimuthal wave

Table 1. Nondimensional Period of Traveling Waves for Different Grid Resolutions

$12\times24\times24$	$16\times32\times32$	$24\times48\times48$	$32\times64\times64$
21.2864	21.0721	21.0170	21.0175

was determined for each mesh, and the results are shown in Table 1. Quite clearly the difference in period between resolutions of $24\times48\times48$ and $32\times64\times64$ is minimal, being of the order of 0.002% of one period. Thus solutions at $32\times64\times64$ are considered sufficiently well resolved, and this is the resolution used for all simulations discussed below.

To check that the converged solutions agree with experiment, the wave speeds for all simulations are compared to the experimental results of Coles (1965). The results are shown in Figure 2, and demonstrate that the flow simulations quantitatively predict this aspect of the experiments and are strong evidence to suggest that the flow solutions are correct. One simulation was also performed to compare to detailed results presented in table 4 of King et al. (1984). For $\eta = 0.868$, $\lambda_z = 2.2$, $Re_I = 687.15$ ($5.97Re_C$), and $m = 6$, a period of $20.378 \pm 2\times10^{-3}$ is predicted here. Values given by King et al. for this flow are $20.434 \pm 6\times10^{-3}$ predicted numerically and $20.44 \pm 1.2\times10^{-2}$ measured experimentally. The prediction here disagrees with the numerical result of King et al. by less than 0.3%. This small discrepancy is most likely a result of the difference in numerical methods, with that in King et al. being the highly accurate spectral method of Marcus (1984).

The integration of fluid-particle trajectories was compared to results by Broomhead and Ryrie (1988). The results (shown in Figure 3) are in excellent agreement and indicate that: (1) the RK4 integration scheme used here is correctly implemented; and (2) discretization of the analytic velocity field introduces no significant error in the final solutions, and therefore the numerical discretization of true wavy vortex flow is unlikely to be a source of significant error.

The results of Coles (1965) suggest that in an inner rotating Taylor–Couette vessel with $\eta = 0.874$, the doubly periodic wavy regime persists until a Reynolds number of approx-

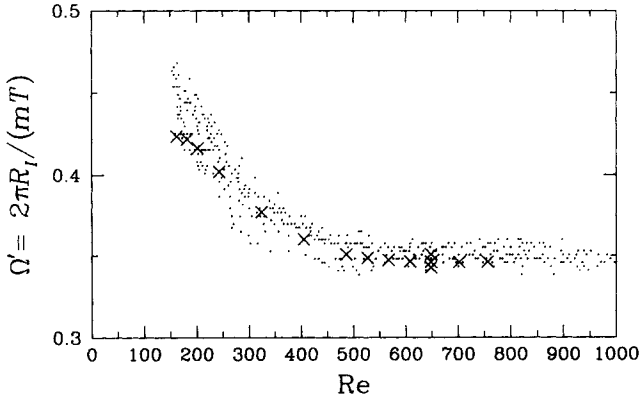

Figure 2. Dimensionless wave velocity of the azimuthal wave for Coles' (1965) experiments (·) and our numerical simulations (×).

The numerical results for one Re_I depend on the wave state (m, n), although they fall fairly closely on top of each other.

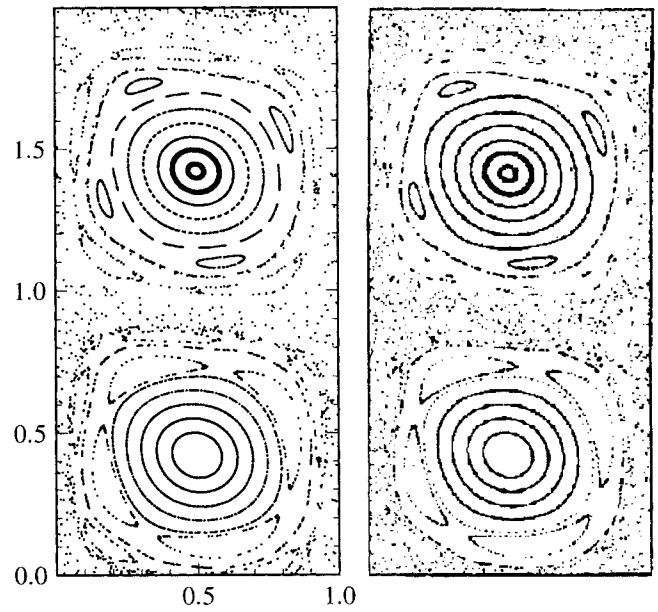

Figure 3. Poincaré sections for the velocity field of Broomhead and Ryrie (1988).

On the left is the map obtained here, and on the right is a representation of that presented in Figure 6b of Broomhead and Ryrie. Courtesy of British Defense Evaluation and Research Agency.

imately 1,300. A range of Reynolds numbers from 162 to 1,296 was initially considered here, although for Reynolds numbers greater than 756 (972 and 1,296 were examined closely), flow solutions with a single azimuthal frequency could not be attained numerically. For both $Re = 972$ and 1,296, a low-frequency component was observed in the velocity spectra. Coles did not measure velocity spectra in his experiments, and the presence of additional, less energetic, azimuthal waves cannot be ruled out. Coles also comments on the presence of subharmonic axial disturbances being consistently observed in one case at $Re \approx 800$. In the experimental study of Fenstermacher et al. (1979) a transient low-frequency component (labeled there as ω_2) was sometimes observed for Reynolds numbers in the range 950–1,430, especially after rapid starts from rest. When this component existed, it was always observed to decay, although the time scale for decay ranged from a few seconds to a few hours. It is possible that the inability to numerically obtain single-wave solutions here for $Re = 972$ and 1,296 may be a manifestation of the same phenomena, and that if the simulations were run for a sufficient (although impractically long) time, this low-frequency signal would similarly disappear. The inability to obtain single frequencies for $Re = 972$ and 1296 is not believed to indicate any inadequacies in the numerical method, although it does retrict the range of Reynolds numbers considered here to 162–756.

Results: Fluid-Particle Trajectories

In axisymmetric Taylor vortex flow, fluid particles are constrained to lie on the surface of the torus on which they start. This is not the case for wavy vortex flow, where fluid particles can be transported in the axial direction. This is clearly demonstrated in Figures 4 and 5, which are Poincaré sections

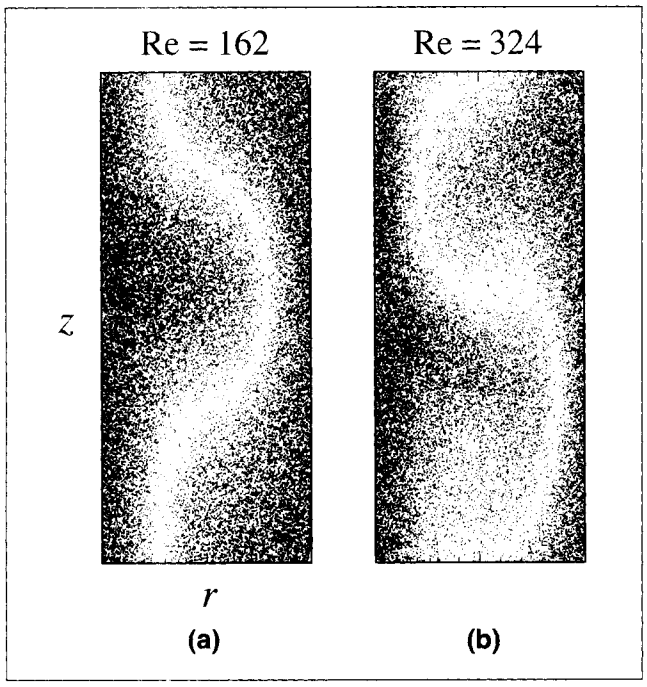

Figure 4. Poincaré maps for two of the wavy vortex flows.

Each has a wave state of (6,12): (a) $Re = 162$, and (b) $Re = 324$. The initial condition was 20 equally spaced points on a vertical line equidistant between the inner and outer cylinders.

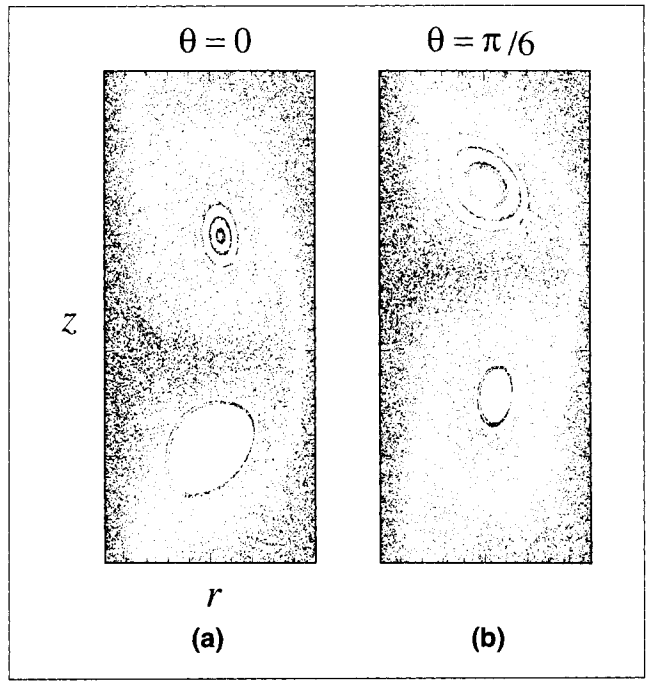

Figure 5. Poincaré sections for wavy vortex flows with a wave state of (a) (6,12) and (b) $Re = 648$ on r-z planes spaced half an azimuthal wavelength apart.

of wavy vortex flow in a coordinate frame corotating with the azimuthal wave. The initial condition is 20 equally spaced particles on a vertical line that is equidistant from the inner and outer cylinders. The axial periodicity of the flow is used to wrap particle trajectories that exit either of the axial boundaries back into the domain. Sections for three Reynolds numbers (162, 324, and 648) are shown for a wave state of (6, 12). The figures clearly show that transport is chaotic in all three cases. For $Re = 162$ and 324 (Figure 4), the trajectories show no obvious signs of KAM invariant surfaces and the entire flow appears to be chaotic. On the other hand, for $Re = 648$ (Figure 5) the presence of invariant surfaces is clearly seen. These two sections are for the same initial conditions plotted on two $r-z$ planes half an azimuthal wavelength apart and indicate how the invariant surfaces change in size as they meander around the azimuth. Particles inside these regions (termed "vortex cores" here) remain trapped and do not communicate with the exterior chaotic flow. This feature of the flow is discussed in more detail later.

Axial dispersion

Following Broomhead and Ryrie (1988), a measure of mixing in wavy vortex flow is defined using an *effective* particle-diffusion coefficient that is estimated on the basis of particle paths. Because particles are constrained to lie between the inner and outer radii of the vessel, and because they will be advected by a mean flow in the azimuthal direction, an axial (z) diffusion coefficient is appropriate. It is defined to be

$$D_z = \lim_{t \to \infty} D_z(t) = \lim_{t \to \infty} \frac{<(z(t) - z_0)^2>}{2t}, \qquad (6)$$

where z_0 is a particle's initial position and $\langle \cdots \rangle$ represents the mean value of the quantity inside the angled brackets. To ensure meaningful results, a large number of particles must be used. For all simulations discussed below, 10,000 particles are randomly distributed throughout the computational domain and their trajectories are calculated in order to estimate diffusion coefficients. In most cases, particle simulations were integrated for a dimensionless time of 2000 (or approximately 46 full rotations of the inner cylinder).

In the flows considered here, if a diffusion coefficient defined by Eq. 6 reaches a finite and nonzero asymptotic value, then the axial transport of fluid elements may be modeled as a diffusion process. Making a connection between D_z and mixing is difficult because large values of D_z do not necessarily imply good mixing. However, the nature of wavy vortex flow is such that it gives rise to rapid and thorough mixing, and D_z is therefore likely to be a quantitative indicator of the mixing effected by the flow.

In axisymmetric Taylor vortex flow, fluid particles that start inside one vortex can never escape that vortex, thus there is no global mixing of fluid by chaotic advection. In that case, $D_z = 0$. A plot of $D_z(t)$ for axisymmetric vortex flow at a Reynolds number of 140 is shown in Figure 6. (The transition to wavy vortex flow occurs at a Reynolds number $Re_W = 143$ for Coles's apparatus.) The initial steady increase in $D_z(t)$ results from the early-time axial motion within each vortex. However, the axial displacements are limited by the size of the vortex, and a steady decay of $D_z(t)$ toward zero eventu-

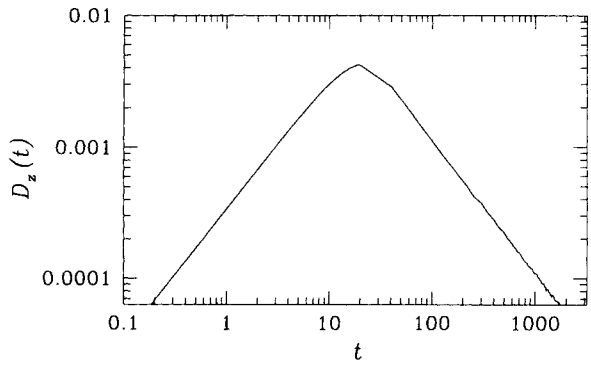

Figure 6. $D_z(t)$ for axisymmetric vortex flow at a Reynolds number of 140, showing the asymptotic behavior for large time.

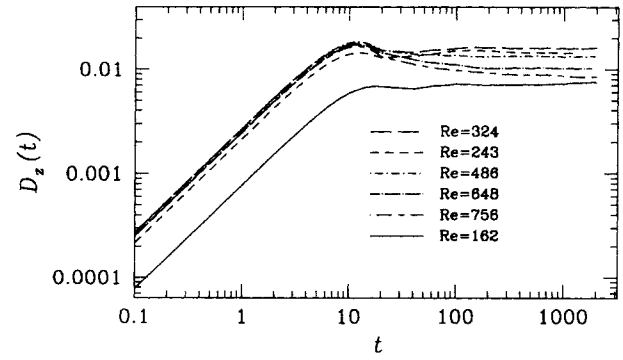

Figure 7. Dimensionless $D_z(t)$ for various Reynolds numbers for a wave state of $(m, n) = (6, 12)$.

To dimensionalize $D_z(t)$, multiply by νRe.

ally results. The results were generated using the particle tracking method detailed earlier with a strictly axisymmetric vortex flow solution. This figure is evidence that particles are not being "diffused" by the numerical method and further indicates the validity of the particle advection technique.

Because the equations have been scaled by the inner cylinder velocity and the gapwidth, d, all times and positions obtained from the simulations are nondimensional times and positions. Hence in the subsequent discussion, $D_z(t)$ is defined as in Eq. 6 and is a *dimensionless* function of the (dimensionless) simulation time t. Thus D_z is the asymptotic dimensionless axial diffusion coefficient. A dimensional diffusion coefficient, $\mathfrak{D}_z$, is obtained by

$$\mathfrak{D}_z = \mathfrak{U} d D_z = \nu Re D_z.$$

Axial dispersion as a function of Re

In previous studies of Taylor–Couette flow, relationships between axial dispersion and Reynolds number have been proposed. For turbulent vortex flow, Tam and Swinney (1987) find that D_z scales like Re_I^{β}, where β depends primarily on the ratio of inner to outer radius, η. In their study β ranged approximately between 0.7 and 0.85 for radius ratios ranging between 0.494 and 0.875. In contrast, Moore and Cooney (1995) suggest that for a wide range of η and flow regimes, including wavy vortex flow, D_z scales like $Re_I^{1.05}$. In a numerical study of modulated wavy vortex flow, Rudman (1995) found that D_z appeared to scale like Re_I for the narrow gap device ($\eta = 0.952$) considered there.

The Reynolds numbers considered here are 162, 182, 202, 243, 324, 408, 486, 527, 567, 608, 648, 702, and 756 for a wave state of $(m, n) = (6, 12)$. This wave state was accessible for all Reynolds numbers reported in Coles' experiments and was numerically found here to result in a well-defined period of oscillation for all Re considered.

The dimensionless $D_z(t)$ derived directly from particle paths are plotted in Figure 7 for a selection of Re. The figure shows the early time increase in $D_z(t)$ as the fluid elements move away from their initial positions. The early increase is followed by a leveling off as t becomes large and $D_z(t)$ asymptotes to a constant value. Nondimensional values of D_z are given in Table 2. As seen there (as well as in Figure 7), D_z is not a monotonic function of Re.

These results may be conveniently displayed by defining an effective Schmidt number (Sc) resulting from chaotic transport:

$$Sc_{\text{eff}} = \nu / \mathfrak{D}_z \tag{7}$$

$$= (Re D_z)^{-1}. \tag{8}$$

Table 2. Nondimensionalized D_z, Nondimensionalized rms Velocity Fluctuations and Sc_{eff} as a Function of Reynolds Number for a Wave State $(m, n) = (6, 12)$*

Re	Re/Re_C	$Dz \times 100$	Sc_{eff}	$\langle U' \rangle \times 100$	$\langle V' \rangle \times 100$	$\langle W' \rangle \times 100$	Core %
162	1.37	0.74	0.846	0.91	4.58	2.39	0.3
182	1.54	1.30	0.423	1.42	6.89	3.83	0.0
202	1.71	1.37	0.361	1.69	7.77	4.57	0.0
243	2.05	1.44	0.284	2.03	8.34	5.40	0.0
324	2.74	1.60	0.193	2.39	8.17	6.02	0.0
405	3.42	1.51	0.164	2.56	7.66	5.95	0.0
486	4.10	1.33	0.154	2.50	7.05	5.47	2.0
527	4.45	1.22	0.156	2.43	6.79	5.19	5.2
567	4.79	1.16	0.152	2.36	6.57	4.93	7.7
608	5.14	1.06	0.152	2.29	6.37	4.68	9.7
648	5.47	1.02	0.151	2.22	6.21	4.46	11.5
702	5.93	0.92	0.155	2.14	6.01	4.19	13.3
756	6.39	0.84	0.155	2.07	5.84	3.95	15.6

*The dimensional values of both D_z and the rms velocity components scale linearly with Re.

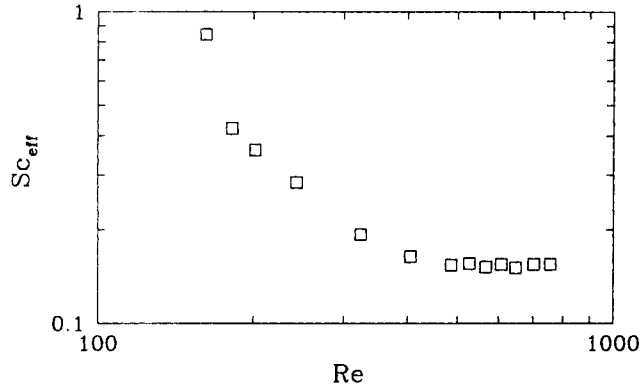

Figure 8. Sc_{eff} as a function of Reynolds number.
Results for a wave state of $(m,n)=(6,12)$.

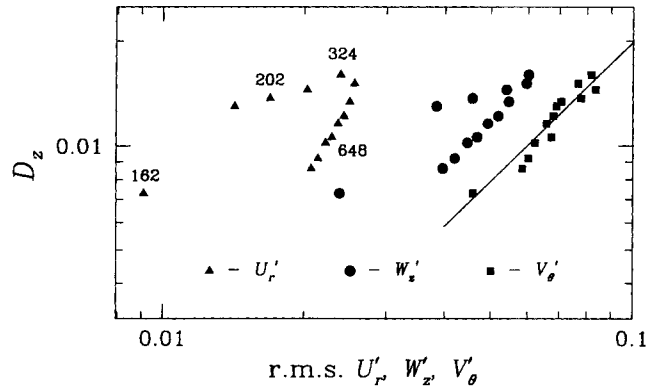

Figure 9. Nondimensional D_z as a function of nondimensionalized rms velocity fluctuations.
Results for a wave state of $(m,n)=(6,12)$.

The effective Schmidt number is plotted in Figure 8 as a function of Reynolds number, and values are also given in Table 2. If a simple power-law scaling between D_z and Re existed for the results here, the Schmidt number could be written

$$Sc_{\text{eff}} \propto Re^{-\lambda}.$$

The relationship between Sc_{eff} and Re is not that of a simple power law, however, and such a parameterization is not possible in wavy vortex flow, even for a fixed wave state.

However, the results do suggest that as Re increases, Sc_{eff} approaches a constant value of approximately 0.155. This indicates that provided a fixed wave state can be maintained, axial dispersion in the wavy vortex regime plateaus and that rotation beyond a certain limit does not lead to faster axial dispersion. It must be remembered that as the rotation is increased, the wave state is unlikely to be maintained and the wavy flow will eventually be modulated with additional frequencies that may influence dispersion significantly.

In their study of time-dependent Rayleigh–Bénard convection, Solomon and Gollub (1988) show that the effective diffusion coefficient in their experiment, $\mathfrak{D}_z$, is linearly dependent on the rms velocity component normal to the diffusion direction (that is, $\mathfrak{U} \times W'$ here). Equivalently, this states that (the nondimensional) D_z is a linear function of the nondimensional rms velocity fluctuations. Root-mean-square velocity fluctuations nondimensionalized with the rotational velocity of the inner cylinder have also been calculated for the flows here (see Table 2), with the mean flow taken to be the azimuthally averaged wavy vortex flow. The nondimensional D_z are plotted as a function of the nondimensionalized rms velocity components in Figure 9.

In this figure, the Reynolds number is marked against selected points for U'. As Re increases from 162, D_z and the nondimensional rms velocity fluctuation monotonically increase up to about $Re = 324$. As Re is increased further, the nondimensional rms velocity fluctuation monotonically decreases, as does D_z. A similar pattern is followed by both V' and W'. The relationship between U' and D_z and that between W' and D_z have a different form for Re less than and greater than approximately 324. Thus D_z is a multivalued function of U' or W', and attempting to fit a power-law relationship, as Solomon and Gollub were able to for W' in their study of Rayleigh–Bénard convection, is not possible here.

Despite the nonmonotonic relationship between D_z and Re, a least-squares fit of the data yields a reasonable power-law fit between D_z and V', which is given by

$$D_z \approx 0.42(V')^{1.3}. \tag{9}$$

This fit is applicable to the wave state $(m,n)=(6,12)$ only.

Effect of wave state

A number of different wave states were examined for several Reynolds numbers—numerically, the largest range of accessible states was found for $Re = 648$ and this case features most prominently. The results are considered in two groups: (1) n fixed with m varying; and (2) m fixed with n varying.

Cases with $n = 12$, m Varying. The effect of varying the azimuthal wave number is shown in Table 3. The results from this rather small sample of data points suggest that for a given Reynolds number, lower azimuthal wave numbers give rise to more rapid axial dispersion. They also correspond to flows

Table 3. Nondimensional D_z, Nondimensional rms Velocity Fluctuations and Sc_{eff} as a Function of Azimuthal Wave Number for $n = 12$

Re	m	$D_z \times 100$	Sc_{eff}	$\langle U' \rangle \times 100$	$\langle V' \rangle \times 100$	$\langle W' \rangle \times 100$	Core %
162	5	1.12	0.519	1.34	6.66	3.04	2.1
	6	0.74	0.846	0.91	4.58	2.39	0.3
648	5	1.15	0.136	2.97	7.43	5.56	4.8
	6	1.02	0.152	2.22	6.21	4.46	11.5
	7	0.88	0.176	1.69	5.12	3.60	16.1

Table 4. D_z, rms Velocity Fluctuations and Sc_{eff} as a Function of Axial Wave Number for $m = 6$*

Re	n	λ_z	$D_z \times 100$	Sc_{eff}	$\langle U' \rangle \times 100$	$\langle V' \rangle \times 100$	$\langle W' \rangle \times 100$	Core %
	12	2.325	0.74	0.846	0.91	4.58	2.39	0.3
162	14	1.993	0.68	0.905	1.14	5.23	2.53	1.0
	16	1.744	0.33	1.851	1.09	4.57	2.06	1.4
	10	2.79	1.86	0.166	2.04	7.84	6.13	0.0
324	11	2.536	1.69	0.182	2.22	8.05	6.11	0.0
	12	2.325	1.60	0.193	2.39	8.17	6.02	0.0
	10	2.79	1.24	0.116	1.81	5.95	4.48	11.6
	11	2.536	1.12	0.138	2.00	6.10	4.46	11.4
648	12	2.325	1.02	0.152	2.22	6.21	4.46	11.5
	13	2.146	0.91	0.170	2.47	6.31	4.49	11.5
	14	1.993	0.86	0.180	2.75	6.42	4.57	10.4
	15	1.86	0.83	0.186	3.07	6.59	4.77	9.4

*The axial wavelength (λ_z) is shown in units of the gapwidth d.

with higher rms velocity components, in agreement with the results found for varying Re. Because of the small sample of points available for a fixed Re and n, it is not possible to postulate a relationship between D_z and rms velocity fluctuations.

Cases with $m = 6$, n Varying. The effect of varying the axial wave number is shown in Table 4, and results for $Re = 324$ and 648 are plotted in Figure 10. For $Re = 162$ the results follow no obvious trend, but for $Re = 324$ and 648 two observations are made. First, for fixed Re, decreasing n (i.e., longer axial wavelengths) is associated with increasing D_z. This is not unexpected because for larger axial wavelengths fluid is transported further in each "vortex" and may be expected to be transported more rapidly. The second observation is that increasing D_z is also associated with decreasing rms velocity fluctuations. This is in contrast to previous results (e.g., the empirical relationship described in Eq. 9) where increasing D_z was associated with increasing rms velocity fluctuations. An explanation of this observation is suggested in the study of Tam and Swinney (1987), who found that D_z is linearly proportional to the axial wavelength λ_z for turbulent Taylor–Couette flow. They also quote the result due to Zeldovich (1982), who found theoretically

$$D \propto \lambda V_{rms} \tag{10}$$

in periodic turbulent flows. Provided W' is used for V_{rms} and λ_z for λ, Eq. 10 fits the data for $Re = 324$ and 648 quite well. The results for either Re have a scatter of less than 3%, although the constant of proportionality slightly differs for each Re. However, because of the small range of data points, and the uncertainty in applicability of Eq. 10 to the laminar chaotic flows here, a definitive parameterization is still lacking.

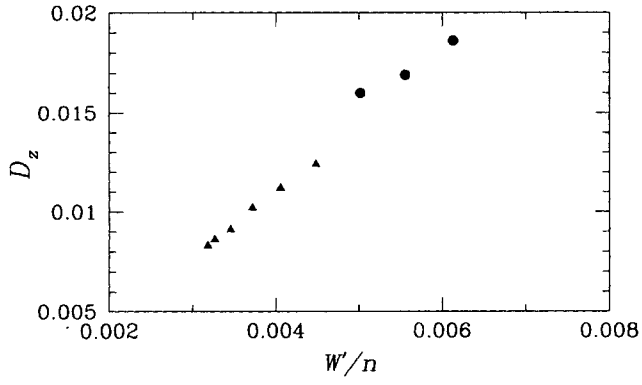

Figure 10. Dimensionless D_z as a function of W'/n (●: $Re = 324$; ▲: $Re = 648$).

Summary of the Effect of Wave State. For the small range of wave states considered here, the effective Schmidt number of wavy vortex flow at $Re = 648$ was seen to vary by a factor of approximately 1.6. At least 20 different wave states are accessible at this Reynolds number, and 1.6 is likely to be a conservative estimate of the range of Sc_{eff}. As a result of this significant variability, the task of finding a functional relationship between Sc_{eff} (or D_z) and Re cannot be attempted without also considering wave state. Although modulating frequencies will quantitatively alter the picture of dispersion and mixing presented earlier, it may be reasonably expected that qualitatively similar behavior will occur in the modulated wavy vortex regime, up until the flow becomes turbulent.

The lack of a clear and consistent relationship between D_z and rms velocity fluctuations for all Reynolds numbers means that predictions of dispersion and/or mixing based on measurable velocity information must await alternative parameterizations. There is a reasonable correlation between D_z and the axial wavelength of the flow as observed by Tam and Swinney (1987) for turbulent flow. A correlation between D_z and azimuthal wavelength cannot be confidently proposed because of the limited number of sample points in m that could be found numerically.

Fluid entrainment

When the symmetry of Taylor vortex flow is broken with a small perturbation, KAM theory predicts that most of the tori on which particle trajectories lie will survive, with those closest to the hyperbolic points on the inner and outer cylinders being the first to become chaotic [see sections 6.10 and 6.11 of Ottino (1989) for a descriptive discussion of this phenomenon]. As the perturbation magnitude increases, more of the tori are destroyed, although other features such as islands and cantori may appear (see, for example, the Poincaré sections in Figure 3). Chaotic particle paths in a nonaxisymmetric Taylor–Couette flow model are predicted in the results of Broomhead and Ryrie (1988), and more recently in the results of Ashwin and King (1997). Ashwin and King cal-

culate particle paths in nonaxisymmetric Taylor–Couette flow using weakly nonlinear asymptotic solutions to the Navier–Stokes equations. Their solutions predict that just after the onset of waviness, most of the axisymmetric tori of Taylor vortex flow survive in a perturbed form and that those tori closest to the cylinder walls become chaotic.

However, what happens to particle trajectories in a fully nonlinear solution of wavy vortex flow far from the transition from two-dimensional axisymmetric Taylor vortex flow has not been reported. Because of limitations in the numerical scheme used here, it has not been possible to examine flow solutions close to the transition ($Re_W \approx 143$). The lowest Reynolds number examined is $Re = 162$, or $1.13Re_W$, thus an important and interesting part of the parameter space cannot be studied here, and results cannot be compared directly to those of Ashwin and King.

For $162 < Re < 405$ in the wavy vortex regime, no observable tori exist and the entire flow appears to be chaotic (see Figure 4). As Re increases above 405, integrable particle trajectories begin to appear, and as Re increases from 486 to 756, the flow volume contained in integrable tori increases. These "wavy vortex cores" are clearly seen in the Poincaré sections displayed in Figure 5. (Note that the position and apparent size of the cores vary with azimuthal position.) In agreement with the results of Ashwin and King (1997), no observable island chains were found in the particle trajectories of wavy vortex flow—where regions of integrable trajectories were found, they appeared to be separated from each other by regions of totally chaotic behavior.

An estimate of the volumetric fraction of the flow that these vortex cores contain was obtained from the particle trajectories and is given by the fraction of the particles that always maintained an axial coordinate within λ_z of their initial position and a radial coordinate that was at least $0.05d$ distant from both cylinders throughout the simulation. Because the axial displacement amplitude of the wavy vortex motion is less than $\lambda_z/4$ in all cases, this measure is sufficient to ensure that particles retained in the core cannot leave numerically, although it is possible that particles that leave the core do not stray far from their initial vortex during the simulation. Thus this retention measure may indicate artificially high retention fractions. The constraint on the radial coordinate was introduced because it was also observed that some particles stayed for considerable lengths of time in stagnation regions near one of the cylinders, thus artificially inflating estimates of vortex core size. To check the reliability of these estimates, several calculations were run for twice as long and the predicted retention fractions were observed to vary only minutely. The statistical variation in the retention results was estimated by running the same simulation several times with different initial particle positions. The retention percentages are estimated to be accurate to $\pm 0.5\%$.

The percentages of particles retained in vortex cores as a function of Re for $(m, n) = (6, 12)$ are shown in the final column of Table 2, and for various wave states in Tables 3 and 4. For the wave state (6, 12), retention drops from 100% at just before the onset of waviness ($Re \approx 143$) to less than 1% at $Re = 162$. Thus at the lowest Reynolds number considered here, most of the flow appears to be chaotic. Zero retention occurs for Re up to approximately 405, which approximately coincides with the maximum nondimensional diffusion coefficient D_z. As Re increases from 405, the retention increases monotonically as D_z decreases, and integrable particle paths begin to appear in the Poincaré sections. The absence of flow solutions in the range $143 < Re < 162$ leaves a gap in the behavior of particle trajectories between axisymmetric flow and fully chaotic flow that awaits further investigation.

A modified diffusion coefficient D_z^M can be defined that is based only on those particles that participate in the global mixing:

$$D_z^M = \frac{100}{100 - P} D_z,$$

where P is the percentage of retained particles. However, taking particle retention into account does little to improve attempts to fit power-law relationships between diffusion coefficients and Re. It does, however, explain at least part of the apparent trend toward a limiting value of Sc_{eff} as Re increases.

For $Re = 648$ and $m = 6$, the retention is fairly uniform at 11% and cannot be an explanation for the way in which D_z varies with n. For $Re = 648$ and $n = 12$, retention is a strong function of m and goes part of the way in explaining the variation of diffusion with m.

Inertial Particle Trajectories

One final study of a preliminary nature is presented here. It arises from the use of Taylor–Couette vessels in studying flocculation reactions (Farrow and Swift, 1996). Because the product of the flocculation reaction is an inertial particle, its subsequent motion after formation is important in attempting to assess the flow conditions to which it has been exposed.

In steady two-dimensional cellular flows, the ability of small inertial particles to settle globally is primarily related to the ratio of convective fluid velocity in the direction of gravity and the nominal particle settling velocity (e.g., Marsh and Maxey, 1985). When the particle settling velocity is higher than the maximum convection velocity, all particles are able to settle. As the ratio of velocities decreases, increasing proportions of particles are entrained inside cell cores—the entrainment regions are termed "retention zones." In axisymmetric Taylor–Couette flow, the picture is more complicated because particles experience a varying centrifugal acceleration in addition to gravitational settling; however, similar particle retention is predicted (Rudman et al., 1994). In wavy vortex flow there is global communication of fluid between vortices, and an expectation of particle entrainment inside vortices cannot be justified *a priori* (see Rudman, 1995). The influence of waviness on inertial particle motion is difficult to estimate, and the aim of this section is to investigate particle dispersion and settling in wavy vortex flow as a function of settling velocity.

Equations of motion

The equations for inertial particles are more complex than Eq. 5, especially if all possible particle forces are to be included (see Maxey and Riley, 1983). Instead of solving the full inertial particle equations here, the particles are assumed

to be sufficiently small that their trajectories are governed by a balance between viscous drag, gravitational force, and fluid stress forces (which include centrifugal, dynamic pressure gradient, and fluid viscous stress forces). In this case, instead of using fluid velocities in the righthand side of Eq. 5, a supplementary set of equations for the particle velocities are solved. The equations are those of Maxey and Riley except that added mass, Basset history, and all terms that are second-order in the particle radius are neglected. Justification for neglecting added mass and history terms is discussed below. Scaling the particle equations with the same scale factors used to nondimensionalize the Navier–Stokes equations allows the inertial particle transport equations to be written in a frame rotating with angular velocity Ω_τ as

$$\frac{dr_p}{dt} = U_p \qquad \frac{d\theta_p}{dt} = \frac{V_p}{r_p} \qquad \frac{dz_p}{dt} = W_p, \tag{11}$$

and

$$\frac{dU_p}{dt} = \frac{V_p^2}{r_p} + 2\Omega_\tau V_p + \Omega_\tau^2 r_p + \frac{1}{\beta}\left[\left(-\nabla P_f + \frac{1}{Re}\nabla^2 U_f\right)_r + \frac{(\beta-1)}{\mathbb{S}Fr^2}(U_f - U_p)\right]$$

$$\frac{dV_p}{dt} = \frac{-U_p V_p}{r_p} - 2\Omega_\tau U_p + \frac{1}{\beta}\left[\left(-\nabla P_f + \frac{1}{Re}\nabla^2 U_f\right)\theta + \frac{(\beta-1)}{\mathbb{S}Fr^2}(V_f - V_p)\right]$$

$$\frac{dW_p}{dt} = \frac{1}{\beta}\left[\left(-\nabla P_f + \frac{1}{Re}\nabla^2 U_f\right)_z + \frac{(\beta-1)}{\mathbb{S}Fr^2}(W_f - W_p) + \frac{(\beta-1)}{Fr^2}\hat{g}\right]. \tag{12}$$

The r-, θ-, and z-components of $\left(-\nabla P_f + \frac{1}{Re}\nabla^2 U_f\right)$ are equal to the righthand sides of Eqs. 1, 2, and 3, respectively. The ratio of particle density to fluid density is $\beta = \rho_p/\rho_f$ and the Froude number is $Fr = \mathfrak{U}/\sqrt{qd}$.

It is convenient to introduce $\mathbb{S} = V_S/\mathfrak{U}$, which is the ratio of the nominal particle settling velocity, V_S, to the velocity of the inner cylinder $\mathfrak{U}$. The nominal particle settling velocity, V_S, is defined to be the Stokes' settling velocity of a single isolated particle in the absence of any liquid flow and depends on the fluid density and viscosity as well as the particle density and radius. For the scaling used here it can be shown that

$$Fr^2 = \frac{2\alpha^2 Re}{9\beta\mathbb{S}}, \tag{13}$$

where α is the ratio of particle radius a to gapwidth d. Rather than define a Froude number here, α, β, and the velocity ratio $\mathbb{S}$ are specified, and the Froude number of the simulation is found from Eq. 13. For all simulations discussed below, values of $\alpha = 0.005$ and $\beta = 2.0$ are used. Keeping both α and β constant and changing $\mathbb{S}$ corresponds physically to changing the viscosity of the liquid and the rotation rate of the inner cylinder in such a way as to maintain the same Reynolds number. Although this makes little sense from an experimental point of view, unreported results suggest that inertial particle settling is only weakly dependent on α and β and is primarily dependent on $\mathbb{S}$. It is this dependence that is investigated here.

The values of α and β used here were chosen as being representative of small mineral particles suspended in a range of fluids typically found in minerals processing applications, in a laboratory-scale Taylor–Couette vessel. From the discussion given in Maxey and Riley (1983) and Liang and Michaelides (1992), a value of $\alpha = 0.005$ gives the ratio of added mass to drag forces as approximately 0.7% and the ratio of history to drag forces as approximately 7%. Neglect of the added mass terms is clearly justified although neglect of the history terms is somewhat more marginal—they are neglected here for ease of computation.

An RK4 time integration is used to integrate Eqs. 11 and 12 forward in time, with quadratic interpolation from the mesh to particle positions. The pressure and fluid viscous stress terms in Eqs. 12 are first differenced on the fluid solution mesh (to cell edge velocity nodes) before interpolation to particle positions.

No good validation cases are available for inertial particle trajectories. Apart from simple tests such as ensuring axial and centrifugal settling velocities were correct for different particle sizes and densities, extensive testing was not undertaken.

Results

Inertial particle trajectories have been calculated for a wave state of (6,12) and a Reynolds number of 648. Six velocity ratios were considered, $\mathbb{S} = 0.001$, 0.0035, 0.01, 0.025, 0.05, and 0.1. A value of $\mathbb{S} = 0.1$ corresponds to a settling velocity that is approximately equal to the maximum axial velocity of the vortex flow. In the case of an axisymmetric vortex flow, almost complete settling of the particles could therefore be expected for $\mathbb{S} = 0.1$ (Rudman et al., 1994).

Each simulation was run with 5,000 randomly distributed inertial particles for a dimensionless time of 2,000. Writing the mean axial coordinate as a function of time as

$$\langle Z(t)\rangle = \frac{1}{N}\sum_{l=1}^{N} z_l(t),$$

the mean settling velocity as a function of time is

$$\langle W(t)\rangle = \frac{1}{t}(\langle Z(t)\rangle - \langle Z(0)\rangle),$$

and an effective diffusion coefficient for inertial particles can be defined relative to the mean axial position

$$D_z = \lim_{t\to\infty} D_z(t) = \lim_{t\to\infty} \frac{\langle (z(t) - z_0 - \langle W(t)\rangle t)^2\rangle}{2t}$$

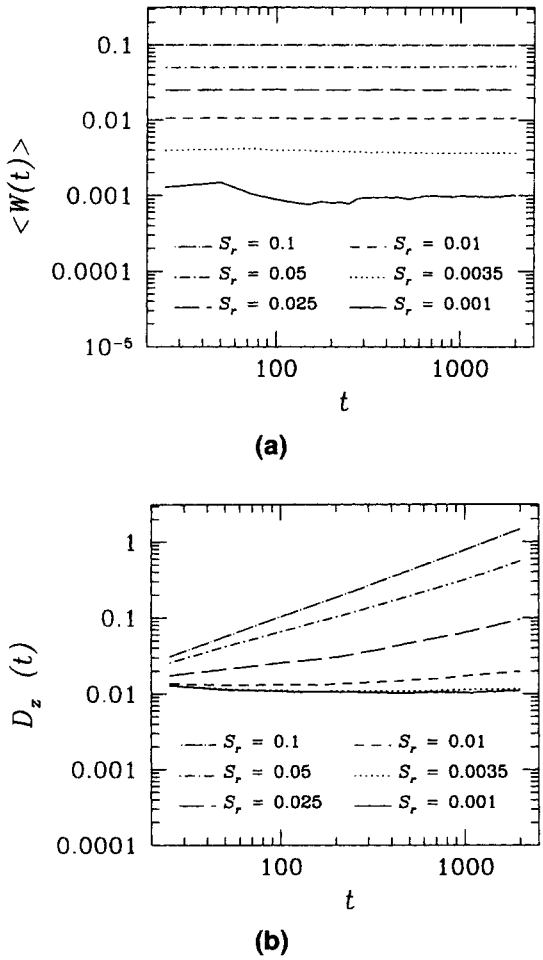

Figure 11. (a) $\langle W(t)\rangle$ vs. t; and (b) $D_z(t)$ vs. t for inertial settling particles.

Figure 11 shows $\langle W(t)\rangle$ and $D_z(t)$ as functions of time. Mean settling velocities are calculated by estimating the average settling over the time interval from $t = 1{,}000$ to 2,000 and are presented in Table 5. Note that $\langle W(t)\rangle$ is fairly uniform over this time (Figure 11a) for all values of $\mathcal{S}$. The result is that on average, small inertial particles in wavy vortex flow settle with a velocity very close to their nominal settling velocity. Although this result is consistent with those found in a preliminary study of modulated wavy vortex flow (Rudman, 1995), it is interesting that centrifugal and other fluid forces arising in vortex flow do not significantly alter mean particle settling.

The effective diffusion of inertial particles is quite similar to fluid particles for low values of $\mathcal{S}$ (approximately $\mathcal{S} < 0.01$). Values of 1.08 and 1.15×10^{-2} are predicted for $\mathcal{S} = 0.001$ and 0.0035 as compared to 1.02×10^{-2} for fluid particles. This result suggests that to a good approximation the ensemble

Table 5. Time-Averaged $\langle W(t)\rangle$ for Inertial Settling Particles as a Function of $\mathcal{S}$ ($m = 6$, $n = 12$, $Re = 648$)

$\mathcal{S}$	0.001	0.0035	0.01	0.025	0.05	0.1
$\langle W\rangle$	0.001	0.00365	0.01068	0.02574	0.05229	0.09088
$D_z\times100$	1.08	1.15	—	—	—	—

axial motion of small inertial particles can be written as an advection diffusion equation. Writing the local axial particle number density as $N(z,t)$, N satisfies

$$\frac{\partial N}{\partial t} + \langle W\rangle \frac{\partial N}{\partial z} = D_z \frac{\partial^2 N}{\partial z^2},$$

where D_z is the effective fluid diffusion coefficient (Eq. 6).

However $D_z(t)$ does not asymptote to a constant value for $\mathcal{S} \geq 0.01$ and increases as t^γ, where the value of γ is dependent on $\mathcal{S}$. This type of behavior is often termed "anomalous diffusion" and has been reported previously in flows with net flux (e.g., Weiss and Knobloch, 1989; Cox et al., 1990). Although the reasons for greater dispersion (at the same time as the mean settling velocity remaining unaffected) are not clear, it is believed that the net consequence of the increasing effects of centrifugal forces is to preferentially move inertial particles into regions of strong up- and downwelling near vortex edges. Although the overall effect of the particles' inertia does not influence mean settling, it has a large impact on dispersion. Important to note in relation to the predicted anomalous diffusion is that the inertial particle velocity field is not divergence-free (and hence not volume preserving), and this behavior is not necessarily surprising.

In summary, faster settling particles disperse more rapidly than the fluid, and their ensemble behavior cannot be modeled using a one-dimensional advection–diffusion equation. Although $D_z(t)$ varies significantly with $\mathcal{S}$, the mean settling velocity remains very close to the nominal settling velocity. These results have implications for residence time distributions of settling particles in wavy vortex flow. They are of a preliminary nature and will be the subject of a more extensive future investigation.

Conclusions

Validated numerical models of wavy vortex flow in a Taylor–Couette vessel and of particle motion in this flow have been presented. The results show that chaotic advection of fluid elements occurs in wavy vortex flow from after the onset of waviness up to the onset of wave modulation. This chaotic fluid motion plays an important role in mixing in these flows, and a measure of mixing can be defined by an axial diffusion coefficient based on axial particle dispersion. For a fixed wave state, the scaled effective diffusion coefficient is not a monotonically increasing function of the Reynolds number, although the true (dimensional) coefficient does monotonically increase for the range of Re investigated. However, it does not increase as any power of Re, as found in the studies of Moore and Cooney (1995) for a wide range of Re, and by Tam and Swinney (1987) for turbulent vortex flow. This suggests that throughflow and/or the nonaxisymmetric outflow in the vessel used by Moore and Cooney have an appreciable effect on chaotic fluid motion in Taylor–Couette flow. The turbulent flow considered by Tam and Swinney is qualitatively different to wavy vortex flow and is almost certainly the cause of the difference in the Reynolds number dependency of the two flow regimes. An effective Schmidt number of the chaotic fluid motion can be defined which, for a wave state of (6, 12), asymptotes to a value of approximately 0.155 for the highest Reynolds numbers studied here. This states that

chaotic advection of fluid elements is an order of magnitude more important for mixing in wavy vortex flow than molecular viscosity.

Not surprisingly, the predicted mixing for a fixed Reynolds number is dependent on the wave state existing in the vessel. Coles (1965) found a large range of accessible wave states (more than 20 for some Reynolds numbers) with transition between states showing considerable hysteresis. For the limited ranges of wave states considered here, Sc_{eff} varied by a factor of 1.6, with states with smaller axial wave numbers (i.e., large axial wavelengths) having a higher effective diffusion. The effective diffusion is also dependent on the azimuthal wave number. There does not appear to be a good relationship between axial diffusion and rms velocity fluctuations across all Reynolds numbers, and a better way of empirically correlating D_z is desirable.

For the higher values of Re considered here, fluid elements were entrained inside vortex cores. The core regions are disconnected from the chaotic flow outside, thus there is an unbroken stream surface separating the inner vortex flow from the exterior flow. Fluid starting inside a vortex core communicates with the exterior flow only by molecular diffusion and does not contribute to the effective diffusion due to chaotic advection. The volume of the core regions decreases from 100% just before the onset of waviness to almost zero by $Re = 162$ (the lowest Re studied here). For $Re > 405$, the percentage of entrained fluid increases again with Re. Although this pattern is consistent with the predicted increase, and then decrease in dimensionless D_z, it cannot fully explain the trend.

An exploratory investigation of the effect wavy vortex flow has on inertial particle settling suggested that the mean settling is not significantly affected by the vortex flow. However, axial dispersion is significantly affected once a particle's nominal settling velocity increases beyond approximately 1% of the rotational velocity of the inner cylinder—which corresponds to about 10% of the axial velocity due to the vortices. The ensemble motion of slower settling particles is well approximated by a one-dimensional advection–diffusion equation, although faster settling particles cannot be described in this manner. These results have implications for particle residence times in Taylor–Couette reactors, but a more complete study is required before definitive statements can be made.

Literature Cited

Amsden, A. A., and F. H. Harlow, "The SMAC Method: A Numerical Technique for Calculating Incompressible Fluid Flows," LASL Rep. LA-4370, Los Alamos, NM (1970).

Andereck, C. D., S. S. Liu, and H. L. Swinney, "Flow Regimes in a Circular Couette System with Independently Rotating Cylinders," *J. Fluid Mech.*, **164**, 155 (1986).

Ashwin, P., and G. P. King, "A Study of Particle Paths in Non-Axisymmetric Taylor-Couette Flow," *J. Fluid Mech.*, **338**, 341 (1997).

Broomhead, D. S., and S. C. Ryrie, "Particle Paths in Wavy Vortices," *Nonlinearity*, **1**, 409 (1988).

Coles, D., "Transition in Circular Couette Flow," *J. Fluid Mech.*, **21**, 385 (1965).

Cox, S. M., P. G. Drazin, S. C. Ryrie, and K. Slater, "Chaotic Advection of Irrotational Flows and Waves in Fluids," *J. Fluid Mech.*, **214**, 517 (1990).

Farrow, J. B., and J. D. Swift, "A New Procedure for Assessing the Performance of Flocculants," *Int. J. Min. Process.*, **46**, 263 (1996).

Fenstermacher, P. R., H. L. Swinney, and J. P. Gollub, "Dynamic Instabilities and the Transition to Chaotic Taylor Vortex Flow," *J. Fluid Mech.*, **94**, 103 (1979).

Hoare, M., T. J. Narendranathan, J. R. Flint, D. Heywood-Waddington, D. J. Bell, and P. Dunhill, "Disruption of Protein Precipitates During Shear in Couette Flow and Pumps," *Ind. Eng. Chem. Fundam.*, **21**, 402 (1982).

Ives, K. J., and M. Al Dibouni, "Orthokinetic Flocculation of Latex Microspheres," *Chem. Eng. Sci.*, **34**, 983 (1979).

Kataoka, K., H. Doi, T. Hongo, and M. Futagawa, "Ideal Plug Flow Properties of Taylor Vortex Flow," *J. Chem. Eng. Jpn*, **8**, 472 (1975).

King, G. P., Y. Li, W. Lee, H. L. Swinney, and P. S. Marcus, "Wave Speeds in Wavy Taylor-Vortex Flow," *J. Fluid Mech.*, **141**, 365 (1984).

Leonard, B. P., "A Stable and Accurate Convective Modelling Procedure Based on Quadratic Upstream Interpolation," *Comp. Meth. Appl. Mech. Eng.*, **19**, 59 (1979).

Liang, L., and E. E. Michaelides, "The Magnitude of Basset Forces in Unsteady Multiphase Flow Computations," *J. Fluid Eng.*, **114**, 417 (1992).

Marcus, P. S., "Simulation of Taylor-Couette Flow. Part 2. Numerical Results for Wavy-Vortex Flow with One Travelling Wave," *J. Fluid Mech.*, **146**, 65 (1984).

Marsh, B. D., and M. R. Maxey, "On the Distribution and Separation of Crystals in Convecting Magma," *J. Volcanol. Geotherm. Res.*, **25**, 95 (1985).

Maxey, M. R., and J. J. Riley, "Equation of Motion for a Small Rigid Sphere in a Nonuniform Flow," *Phys. Fluids*, **26**, 883.

Moore, C. M. V., and C. L. Cooney, "Axial Dispersion in Taylor-Couette Flow," *AIChE J.*, **41**, 723 (1995).

Morton, D. E., M. J. Rudman, and J.-L. Liow, "Numerical Simulation of Splashing Phenomena," *Proc. Int. Conf. on Numerical Methods in Laminar and Turbulent Flow*, C. Taylor and P. Durbetaki, eds., Atlanta, GA, p. 1007 (1995).

Ottino, J. M., "The Kinetics of Mixing: Stretching, Chaos and Transport," chap. 1, Cambridge Univ. Press, Cambridge (1989).

Pudjiono, P. I., and N. S. Tavare, "Residence Time Distribution Analysis from a Continuous Couette Flow Device Around Critical Taylor Number," *Can J. Chem. Eng.*, **71**, 312 (1993).

Pudjiono, P. I., N. S. Tavare, J. Garside, and K. D. P. Nigam, "Residence Time Distribution from a Continuous Couette Flow Device," *Chem. Eng. J.*, **48**, 101 (1992).

Rudman, M. "Mixing in the Wavy Vortex Regime of Taylor-Couette Flow," *Proc. Australasian Fluid Mechanics Conf.*, R. W. Bilger, ed., Sydney, Australia, p. 291 (1995).

Rudman, M., M. C. Thompson, and K. Hourigan, "Particle Shear-Rate History in a Taylor-Couette Column," *Liquid-Solid Flows*, M. C. Rocco, C. T. Crowe, D. D. Joseph, and E. E. Michaelides, eds. ASME FED, Vol. 189, ASME, New York, p. 22 (1994).

Ryrie, S., "Mixing by Chaotic Advection in a Class of Spatially Periodic Flows," *J. Fluid Mech.*, **236**, 1 (1992).

Solomon, T. H., and J. P. Gollub, "Chaotic Transport in Time-Dependent Rayleigh-Bénard Convection," *Phys. Rev. A*, **38**, 6280 (1988).

Stein, H. N., E. H. Logttenberg, A. J. G. VanDieman, and P. J. Peters, "Coagulation of Suspensions in Shear Fields of Different Characters," *Colloids Surf.*, **18**, 223 (1986).

Tam, W. Y., and H. L. Swinney, "Mass Transport in Turbulent Couette-Taylor Flow," *Phys. Rev. A*, **36**, 1374 (1987).

Taylor, G. I., "Stability of a Viscous Liquid Contained Between Two Rotating Cylinders," *Philos. Trans. R. Soc. London Ser. A*, **223**, 289 (1923).

Tsai, C., S. Iacobellis, and W. Lick, "Flocculation of Fine-Grained Lake Sediments Due to a Uniform Shear Stress," *J. Great Lakes Res.*, **13**, 135 (1987).

Weiss, J. B., and E. Knobloch, "Mass Transport and Mixing by Modulated Travelling Waves," *Phys. Rev. A*, **40**, 2579 (1989).

Welch, J. E., F. H. Harlow, J. P. Shannon, and B. J. Daly, "The MAC Method. A Computing Technique for Solving Viscous, Incompressible, Transient Fluid-Flow Problems Involving Free Surfaces," LANL Rep. LA-3425, Los Alamos, NM (1965).

Zeldovich, Y. B., *Sov. Phys.—Dokl.*, **27**, 797 (1982).

Manuscript received Aug. 12, 1997, and revision received Feb. 13, 1998.